Journal of Colloid and Interface Science 585 (2021) 337–346

Contents lists available at ScienceDirect

Journal of Colloid and Interface Science

journal homepage: www.elsevier.com/locate/jcis

Regular Article

Molecular dynamics simulation of the adsorption of per- and polyfluoroalkyl substances (PFASs) on smectite clay

Jennifer A.R. Willemsen *, Ian C. Bourg

Department of Civil & Environmental Engineering and High Meadows Environmental Institute, Princeton University, Princeton, NJ 08544, United States

GRAPHICAL ABSTRACT

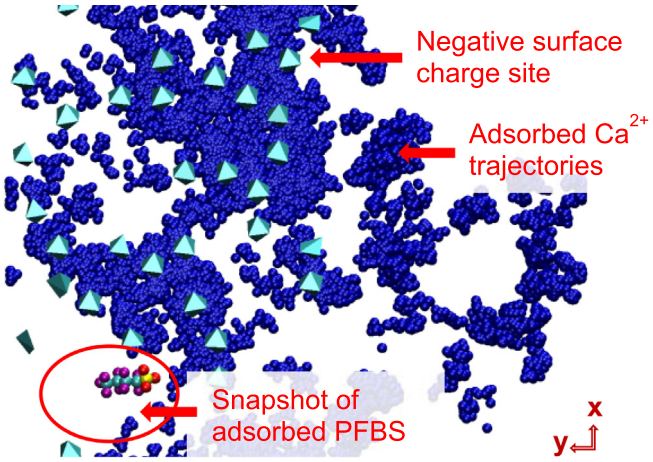

ARTICLE INFO

Article history:
Received 22 September 2020
Revised 6 November 2020
Accepted 19 November 2020
Available online 24 November 2020

Keywords:
Per- and polyfluoroalkyl substances
Clay mineral geochemistry
Smectite
Molecular dynamics
Metadynamics
Adsorption
Emerging organic contaminants

ABSTRACT

Molecular dynamics (MD) simulations are used to predict the partitioning of per- and polyfluoroalkyl substances (PFASs) to smectite clay, a high surface area adsorbent ubiquitous in temperate soils. Simulated systems model a stack of flexible smectite lamellae in contact with a bulk aqueous reservoir containing PFAS molecules. Perfluorobutanesulfonic acid (PFBS), perfluorohexanesulfonic acid (PFHxS), and perfluorooctanesulfonic acid (PFOS) are simulated at various aqueous chemistry conditions to examine the effect of PFAS size, salinity, and coordinating cation type (K^+, Na^+, and Ca^{2+}) on adsorption. The metadynamics technique is employed to facilitate the exploration of the simulation cell and to reconstruct the underlying free energy landscape. Adsorption is favorable on the hydrophobic domains of the external basal surfaces with the fluorinated chain adopting a flat orientation on the surface. Analysis of the adsorption energetics reveals large favorable entropic contributions to adsorption. The enthalpy of adsorption is unfavorable, though much less so in the presence of Ca^{2+} due to stabilizing 'lateral cation bridging' interactions between divalent cations and PFAS sulfonate head groups. Overall, this research advances the mechanistic understanding of PFAS-smectite interactions and provides new insights that could help inform fate and transport models and the development of adsorbents and remediation techniques.

* Corresponding author.
E-mail address: jarw@princeton.edu (J.A.R. Willemsen).

https://doi.org/10.1016/j.jcis.2020.11.071
0021-9797/

1. Introduction

The environmental prevalence of per- and polyfluoroalkyl substances (PFASs), a group of persistent, bioaccumulative chemicals, presents an ongoing threat to human health as exposure has been linked to endocrine disruption [1], carcinogenecity [2,3], immunotoxicity [4,5], and developmental impacts [6,7]. These chemicals, first produced in the mid-twentieth century, are widely used in industrial and household products [8] and detected in the serum of 98% of humans tested [9]. Multiple bans and regulations have been placed on the use of certain long-chain PFASs, particularly over the last few years, due to emerging evidence of widespread contamination [10]. However, the continuous development of alternative PFASs, many with their own potentially harmful health effects [11,12], makes the study and remediation of these compounds an ongoing and evolving challenge. Common PFAS exposure pathways include contaminated food, dust, air, and drinking water [13,14]. Contaminated drinking water is of particular concern as conventional water and wastewater treatment approaches are only partially effective for PFAS removal due to the low volatility, high solubility, and high mobility of these contaminants and their moderate affinity for traditional adsorbents [15]. Throughout the United States, drinking water levels of perfluorooctanesulfonic acid (PFOS) and perfluorooctanoic acid (PFOA), historically two of the most widely used PFASs, were found to be above the Environmental Protection Agency's 70 ng/L lifetime health advisory for combined exposure for 6 million residents [16].

A central process governing the fate and transport of organic contaminants in the aquatic environment (and, also, their removal by synthetic adsorbents during water treatment) is their affinity for solid surfaces as characterized by the partition coefficient $K_d = q/C$, where q and C are the concentrations of the contaminant on the adsorbent (mol kg adsorbent^{-1}) and in solution (mol L^{-1}) [17,18]. Adsorption of organic contaminants in soils and sediments has historically been modeled as the sum of adsorption by the soil organic matter (SOM) and clay fractions as these phases account for the majority of accessible surface area in soils [19]. For PFASs specifically, results of soil and sediment adsorption studies have been generally interpreted as indicating that SOM and clay are roughly equally important adsorbents [20–22]. Given the uncertainty in SOM characterization [23,24], attempts to gain further mechanistic insight have typically focused on characterizing PFAS adsorption by pure phase adsorbents. These studies have predominately focused on adsorption by minerals, particularly smectite [25–29], kaolinite [22,25–28,30], and Al- and Fe-oxides [22,28,31,32]. For PFOS, one of the most commonly studied PFASs, measured partition coefficients for adsorption by smectite clay minerals (log K_d = 0.7–3.5) [25,28,29] are commensurate with or greater than those reported for adsorption in soils and sediments (log K_d = 0.1–1.9) [20–22,33,34], suggesting the potential importance of mineral contributions.

Many questions remain regarding the fundamental mechanisms of PFAS adsorption by mineral surfaces as numerous factors have been shown to affect the magnitude of adsorption. These include changes in aqueous chemistry (e.g. salinity, the ratio of divalent to monovalent cations, pH) and structural differences between PFAS molecules (e.g. chain length, hydrophobicity, and head group identity) [22,25,28–32]. Studies of PFAS adsorption in soils have often postulated that interactions with soil organic matter are predominantly hydrophobic in nature, whereas interactions with minerals are predominantly electrostatic [20,22,25,35]. However, this interpretation conflicts with the studies of adsorption on pure mineral phases, according to which PFAS adsorption by minerals is sensitive to both electrostatic and hydrophobic interactions [21,36]. In the case of PFAS interactions with smectite clay minerals specifically, repulsive electrostatic interactions are expected between the anionic PFAS molecules and the negatively charged clay surface as well as between individual adsorbed PFAS molecules [30], while favorable electrostatic interactions are expected between the PFAS molecules and the exchangeable cations coordinating the clay surface [37]. In addition, the siloxane surface of smectite is known to carry uncharged patches (due to the random distribution of isomorphic substitutions) that are capable of forming hydrophobic interactions with non-polar contaminant moieties [38,39] such as the fluoroalkyl tail of PFASs. Although several conceptual models have been proposed to understand the energetics of PFAS adsorption [30,31], there remains a strong need for more mechanistic insight into these energetics, in particular to help enable the development of improved treatment technologies [40,41].

Previous studies of PFAS adsorption have relied largely on a variety of experimental techniques including batch adsorption experiments, X-ray diffraction (XRD), and Fourier transform infrared (FTIR) spectroscopy. While these techniques provide valuable information about the extent of adsorption and molecular conformation when adsorbed, they inherently cannot quantify the influence of different interatomic interactions on the overall free energy of adsorption. Molecular dynamics (MD) simulations have the potential to help deconvolute the energetics of adsorption and thereby promote deeper fundamental understanding of contaminant-mineral interactions. To date, most MD simulations of organic contaminant adsorption have probed relatively short time scales (~0.1–2 ns) that enable characterizing selected molecular configurations and quantifying the associated potential energies of adsorbed molecules, but that do not enable predicting the free energy of adsorption [19,35,42–49]. A handful of simulation studies have used longer simulation times and methodologies adapted to quantify the free energy of organic adsorption, but these studies relied on relatively simplified systems that enabled analyzing adsorption along a single reaction coordinate such as the distance from an infinite clay lamella or location within a nanopore [50–52]. Finally, very few of the studies outlined above examined the adsorption of PFASs on any solid [35].

Here, we build upon advances in high-performance computing, the development of techniques capable of reconstructing complex free energy landscapes [53–56], and the validation of interatomic potential models for the structure and dynamics of water-salt-clay systems [57–61], the combination of which allows for larger and longer simulations capable of quantifying the free energy of adsorption of organic contaminants on more complex surfaces with a variety of coordination environments. Specifically, we use a metadynamics-based MD simulation methodology designed to evaluate the partitioning of organic contaminants from a bulk aqueous reservoir to a stack of flexible smectite clay lamellae [39]. We recently developed and validated this methodology in the case of the adsorption of phthalate esters on smectite clay surfaces at a single aqueous chemistry condition. We now apply it to gain insight into the adsorption of three PFASs of increasing chain length—perfluorobutanesulfonic acid (PFBS), perfluorohexanesulfonic acid (PFHxS), and PFOS—by Ca-, K-, and Na- smectites at different salinities to determine how perfluoroalkyl chain length and aqueous chemistry affect PFAS adsorption. For each system, we quantify the energetics of adsorption, evaluate the role of clay surface charge density, and analyze the observed molecular adsorption conformations.

2. Methods

Most of the methodological details of the present study are described in Willemsen et al. (2019) and are only briefly restated

below. In short, periodically replicated MD simulation cells were constructed to examine PFAS partitioning to Ca-, K-, and Na- smectite (Fig. 1). All simulations contained a stack of two flexible smectite clay lamellae each 9.4 Å thick, 45.7 Å wide, and 63.4 Å deep (essentially infinite given the periodic boundary), corresponding to 60 smectite unit cells. Octahedral Al^{3+} to Mg^{2+} isomorphic substitutions were randomly distributed in the two clay sheets in accordance with Löwenstein's avoidance rule. This resulted in the upper and lower clay lamellae having surface charge densities of 0.60 and 0.55 structural charges per unit cell respectively, near the lower end of the range of reported values [62]. The system was hydrated with 6114 water molecules and the interlayer spacing between the two lamellae was initially set to 6 Å, consistent with a two-water hydrate. Ion pairs were added to the aqueous phase to examine the influence of salinity and cation type on adsorption. Specifically, five distinct aqueous chemistry conditions were simulated: 0.1 M KCl, 0.1 M $CaCl_2$, and 0.009 M, 0.1 M, and 1.0 M NaCl. Three PFAS molecules and charge balancing cations were added to each system. Adsorption of PFBS was simulated at all five aqueous chemistry conditions described above, while PFHxS and PFOS were studied only at 0.1 M $CaCl_2$.

Metadynamics-based simulations were performed to obtain two-dimensional maps of adsorption free energy in our simulated system in order to calculate the partition coefficients of the organic solutes. Additional unbiased simulations were carried out to evaluate the enthalpy of adsorption and analyze adsorption mechanisms. Simulations were run using the LAMMPS program [63] with the Colvars package [64] on the Cori supercomputer at the National Energy Research Scientific Computing Center (NERSC). Interatomic interactions were modeled using the CLAYFF model for clay atoms [65], CLAYFF-compatible parameters for the cleaved smectite edges [66], the OPLS-AA model for PFAS molecules [67,68], the SPC/E model for water molecules [69], and established models for Ca^{2+}, K^+, Na^+, and Cl^- ions [70–72]. All force field parameters are reported in the Supporting Information. Short range Van der Waals (VdW) and Coulomb interactions were solved up to 12 Å; Coulomb interactions beyond this cutoff were solved using the particle–particle/particle-mesh (PPPM) Ewald summation method with 99.9% accuracy [73]. Water molecules were kept rigid using the SHAKE algorithm [74]. To prevent the clay particles from drifting, one clay lamella was tethered in place with its rotational and translational velocity set to zero at each time step. The second lamella was similarly constrained with the exception of translation in the z-direction of the simulation cell, thus allowing the interparticle distance to vary. Beyond the constraints noted above, the clay particles were modeled as fully flexible.

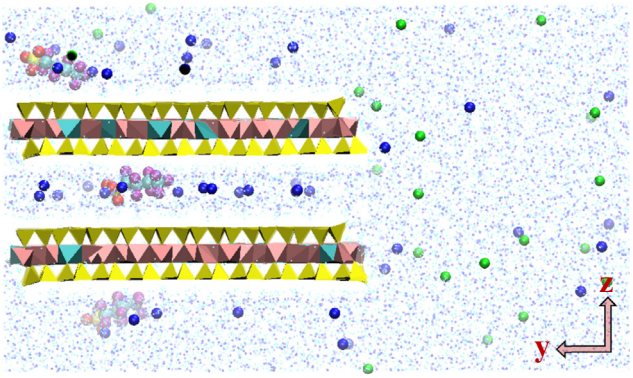

Fig. 1. Simulation snapshot containing two clay lamellae, three PFBS molecules (purple, light blue, yellow and red spheres), calcium ions (dark blue spheres), chloride ions (green spheres), and water molecules (small blue spheres). (For interpretation of the references to colour in this figure legend, the reader is referred to the web version of this article.)

Simulations were equilibrated for 445 ps, including 200 ps in the NP_yT ensemble (P = 1.0 bar) yielding an average simulation cell size of 63.36 Å × 81.18 Å × 46.80 Å with small variations in the y dimension (up to 1.2 Å from the average) between systems due to differences in aqueous chemistry. Following equilibration, production runs were performed at 298 K in the NVT ensemble for up to 95 ns in the case of the unbiased simulations and up to 390 ns for the metadynamics simulations. Metadynamics was performed independently on each of the three PFAS molecules in the simulation cell (allowing for statistical error calculations) using two reaction coordinates: the y- and z-coordinates of the center of mass of the PFAS molecule. A full compilation of the metadynamics simulation parameters for each system can be found in the Supporting Information. Metadynamics simulations were considered complete upon convergence of the three molecular replicates to similar free energy landscapes and stabilization of the free energy difference between the bulk water and clay regions.

Metadynamics simulation results were output for each PFAS molecule every 5 ns. To calculate overall water-clay partition coefficients, data from the last 50 ns of each run were temporally and spatially averaged over a 10 Å × 46.8 Å bulk water region and a 30 Å × 46.8 Å clay region (corresponding to the middle section of the clay lamellae, to avoid edge effects). Region-specific adsorption coefficients were calculated for the interlayer region (6 Å × 46.8 Å) and regions within 6 Å of the upper and lower external basal surface. The equations used to convert the two-dimensional free energy map into a single value of the free energy of adsorption on the entire clay stack or in different regions of the clay stack are described in the Supporting Information and in Willemsen et al. (2019). Since the simulations were performed in the NVT ensemble, reported free energy values represent Helmholtz free energies. They are essentially equivalent to Gibbs free energies, as the inclusion of the NP_yT equilibration step at P_y = 1 bar makes the pressure–volume term relating the Helmholtz and Gibbs free energies negligible.

As noted above, in addition to our metadynamics simulations, we carried out standard ('unbiased') MD simulations of the same systems. Enthalpies of adsorption were calculated from the average VdW and Coulomb interactions between PFAS molecules and all other atoms in the system over the last 90 ns of these simulations. Finally, entropic contributions to adsorption were estimated from the difference between the free energies and enthalpies of adsorption calculated using the metadynamics and unbiased simulations, respectively. Simulation results were analyzed using in-house Matlab routines and visualized using the VMD program [75].

3. Results and discussion

3.1. Metadynamics results and partition coefficient calculations

The two-dimensional (yz) free energy maps revealed by the metadynamics simulations are shown in Fig. 2 for PFBS adsorption under all five aqueous chemistry conditions. Relative to the bulk aqueous region, the results indicate the existence of free energy minima on the lower clay basal surface and little to no affinity for the interlayer nanopore, edge surfaces, and upper basal surface.

Calculated partition coefficients for adsorption on the entire clay stack and in individual sub-domains (upper and lower basal surfaces and interlayer nanopore) are shown in Table 1. Predicted log K_d values were influenced by cation type and increased in the order $Na^+ < K^+ < Ca^{2+}$. The strong enhancement in the presence of calcium is consistent with previous experimental observations on the adsorption of organic anions on smectite [76–78] and is generally interpreted as reflecting the importance of the so-called 'cation bridging' phenomenon, whereby a divalent cation forms a bridge

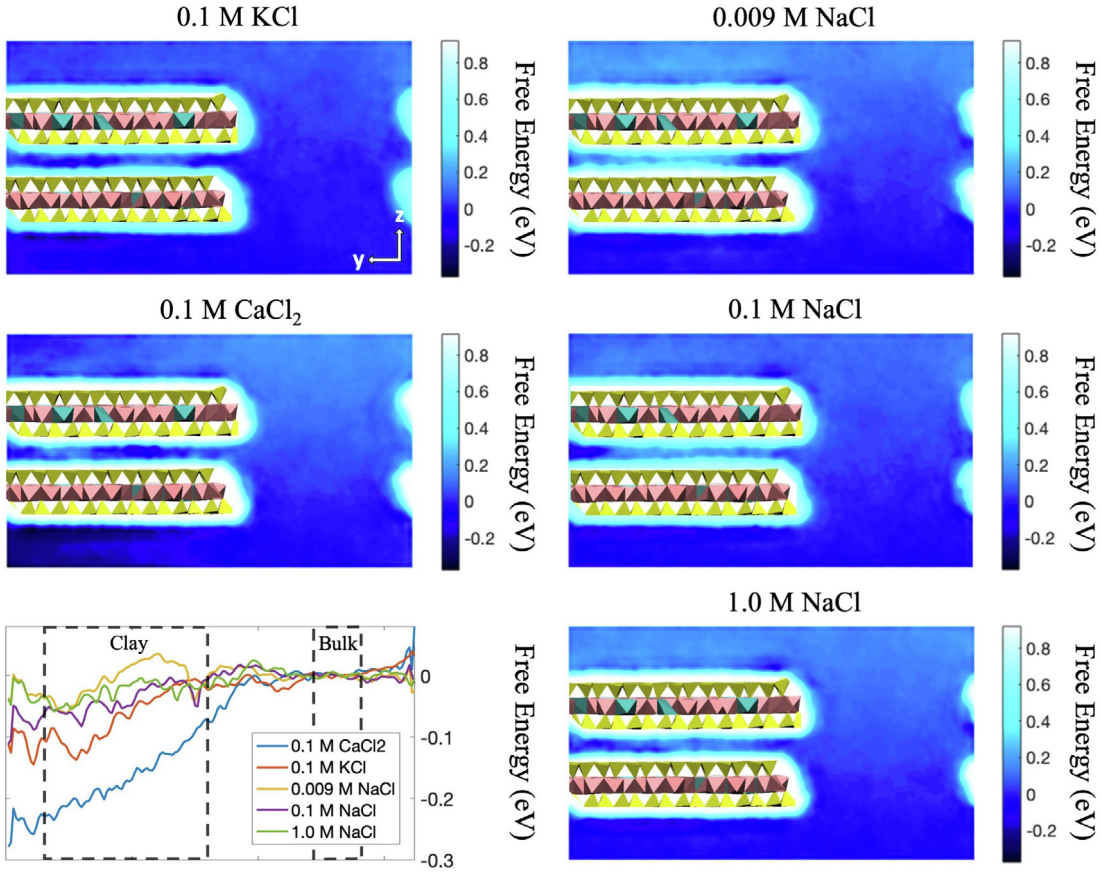

Fig. 2. Metadynamics predictions of the two-dimensional (*yz*) free energy maps for PFBS adsorption on the stack of two smectite lamellae in 0.1 M KCl, 0.1 M $CaCl_2$, 0.009 M NaCl, 0.1 M NaCl, and 1.0 M NaCl electrolyte solutions. Reported free energies are normalized to the average value in the bulk aqueous region. Darker blue regions indicate free energy minima. The lower left panel shows the average free energy profiles as a function of *y* for all systems. The regions outlined in dashed black lines were used to calculate K_d values as described in the Supporting Information and in Willemsen et al. (2019). (For interpretation of the references to colour in this figure legend, the reader is referred to the web version of this article.)

Table 1
Predicted log K_d values (L kg^{-1}) for PFBS adsorption in 0.1 M KCl, 0.1 M $CaCl_2$, 0.009 M NaCl, 0.1 M NaCl and 1.0 M NaCl. Results reported as '*NA*' indicate that the free energy of adsorption was unfavorable (i.e., the solute is negatively adsorbed relative to water).

Salinity	log K_d (predicted)			
	Overall	Lower Surface	Interlayer	Upper Surface
0.1 M KCl	1.3 ± 0.3	1.9 ± 0.5	*NA*	*NA*
0.1 M $CaCl_2$	2.9 ± 0.4	3.5 ± 0.4	0.3 ± 0.2	*NA*
0.009 M NaCl	*NA*	−0.1 ± 0.04	*NA*	*NA*
0.1 M NaCl	0.5 ± 0.4	1.1 ± 0.4	*NA*	*NA*
1.0 M NaCl	0.6 ± 0.6	1.2 ± 0.6	*NA*	*NA*

between two negatively charged functional groups (e.g., a negatively-charged surface site and a carboxylate or sulfonate group) [79–82]. The stronger adsorption in the presence of K^+ than Na^+ likely reflects the lower hydration energy of K^+, which is thought to lessen the obstruction of potential hydrophobic adsorption domains by adsorbed K^+ [48,83,84]. Finally, our results at the three tested sodium salinities show evidence of increasing PFBS adsorption with increasing salinity (0.009 M < 0.1 M ≈ 1.0 M) as expected from previous experimental studies of PFOS adsorption on negatively charged surfaces [25,28]. The lack of a strong interlayer adsorption does limit the number of favorable adsorption domains, but given the nanomolar range of reported PFAS concentrations in the environment [85] and the very high specific surface area of smectite, the exterior surfaces should be sufficient to accommodate contaminant molecules.

3.2. Effects of surface charge density

In all cases, adsorption was dominated by partitioning to the lower basal surface, which only differs from the upper one in the number and distribution of isomorphic substitutions (0.094 C/m^2 vs. 0.103 C/m^2). This suggests that PFBS adsorption on smectite is highly sensitive to charge density, as previously observed in studies of uncharged polar compounds on smectite clay [39,86]. To further investigate this effect, we calculated two-dimensional (*xy*) maps of PFBS density within 6 Å of the basal surfaces in our unbiased simulations. Results for the lower basal surface at our five aqueous chemistry conditions are shown in Fig. 3 along with the location of the isomorphic substitutions in the underlying clay lamella. For solutions containing monovalent cations, PFBS density is almost exclusively concentrated on the largest uncharged (i.e.,

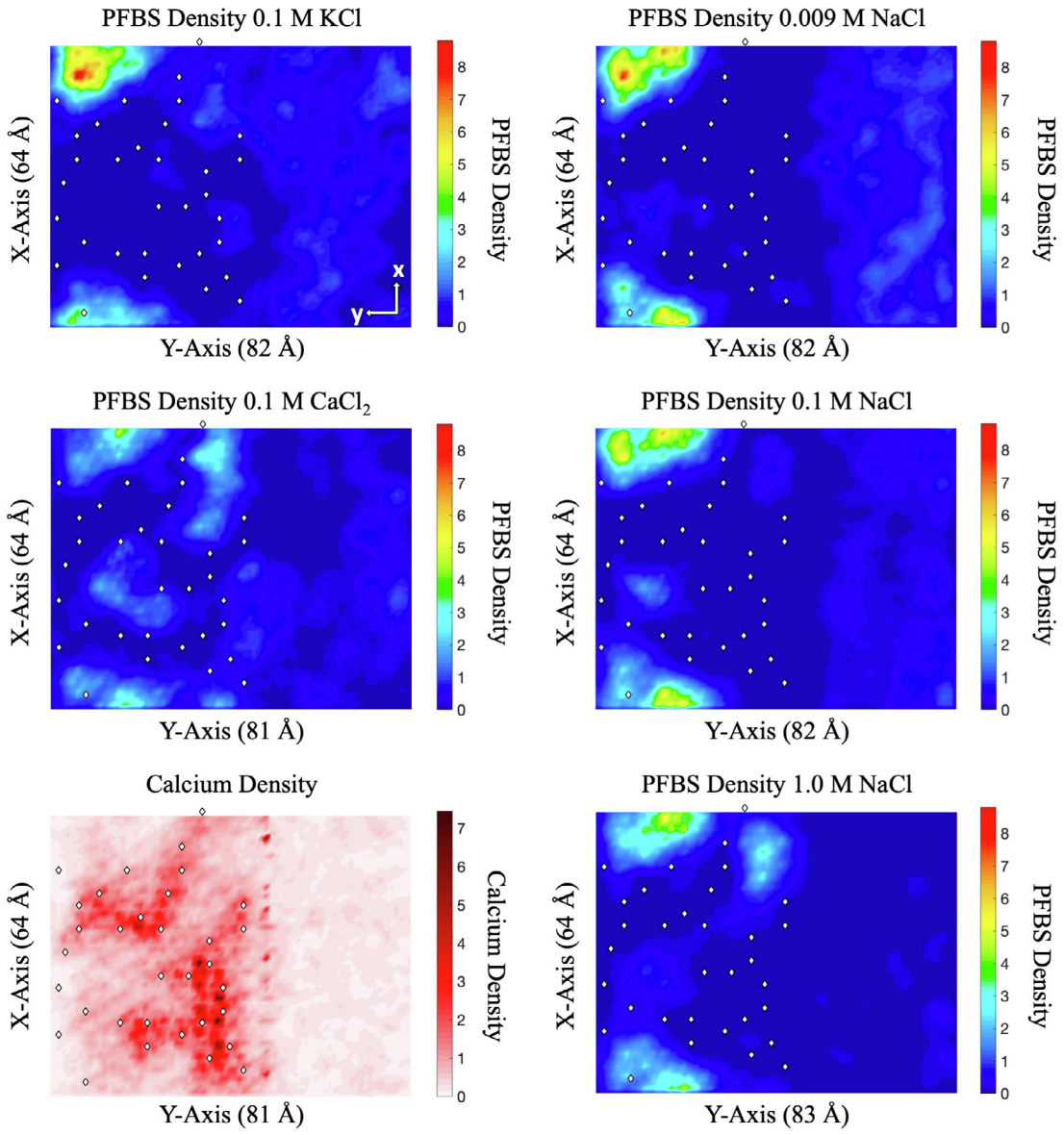

Fig. 3. PFBS density maps in the *xy* plane within 6 Å of the lower basal surface (left side of each map) and in the corresponding bulk-liquid-like water region (right side of each map) in our unbiased simulations. White diamonds represent the location of the isomorphic substitutions in the underlying clay lamella. In each map, PFBS density was scaled to its average value in the region above the lower basal surface (i.e., densities >1 represent portions of the surface with higher than average affinity for PFBS at each aqueous chemistry condition). The lower left panel shows calcium ion density within 6 Å of the lower clay lamella. Density was scaled to its average value in the region above the lower basal surface and as expected, greater Ca^{2+} density is observed in the vicinity of the isomorphic substitutions.

isomorphic substitution free) region of the surface, where the density of adsorbed surface cations is lowest. Previous research has long hypothesized [38,87] and recently confirmed [39,88] the inherent hydrophobicity of the smectite basal surface in the absence of cations and the existence of a strong hydrophobic partitioning of uncharged organic solutes on uncharged portions of this surface. The results presented in Fig. 3 demonstrate that this hydrophobic partitioning on uncharged surface patches also drives the adsorption of PFBS. Our results further reveal that the details of this partitioning are strongly modulated by aqueous chemistry, likely because of the anionic nature of PFBS. Notably, the density maps show that the presence of Ca (and, to a smaller extent, K or a high concentration of Na) enables non-negligible adsorption not only on the largest uncharged patch, but also on smaller uncharged patches closer in proximity to charged regions. The ability of these smaller patches to accommodate PFBS molecules in the presence of $CaCl_2$ suggests the importance of favorable 'lateral' Coulomb interactions between the SO_3^- group of the adsorbed PFBS molecule and the charge balancing Ca^{2+} ions located above charged isomorphic substitutions.

3.3. Coordination of adsorbed PFBS molecules

Atomic density profiles for PFBS, water, and ions near the clay surface are shown in Fig. 4A for the unbiased simulation of the system at 0.1 M $CaCl_2$. On the external basal surfaces, there are sharp carbon density peaks ~2.5 Å from the surface and alternating fluorine peaks ~1.5 Å and ~3.5 Å from the surface. These results indicate that the CF chain displaces water molecules from the first clay hydration layer and lies flat on the mineral surface, an orientation that minimizes interactions between the hydrophobic CF chain and water molecules. The more hydrophilic SO_3^- group has density peaks ~4.5 Å from surface, indicating that it is oriented away from the clay surface. For PFBS in the $CaCl_2$ system,

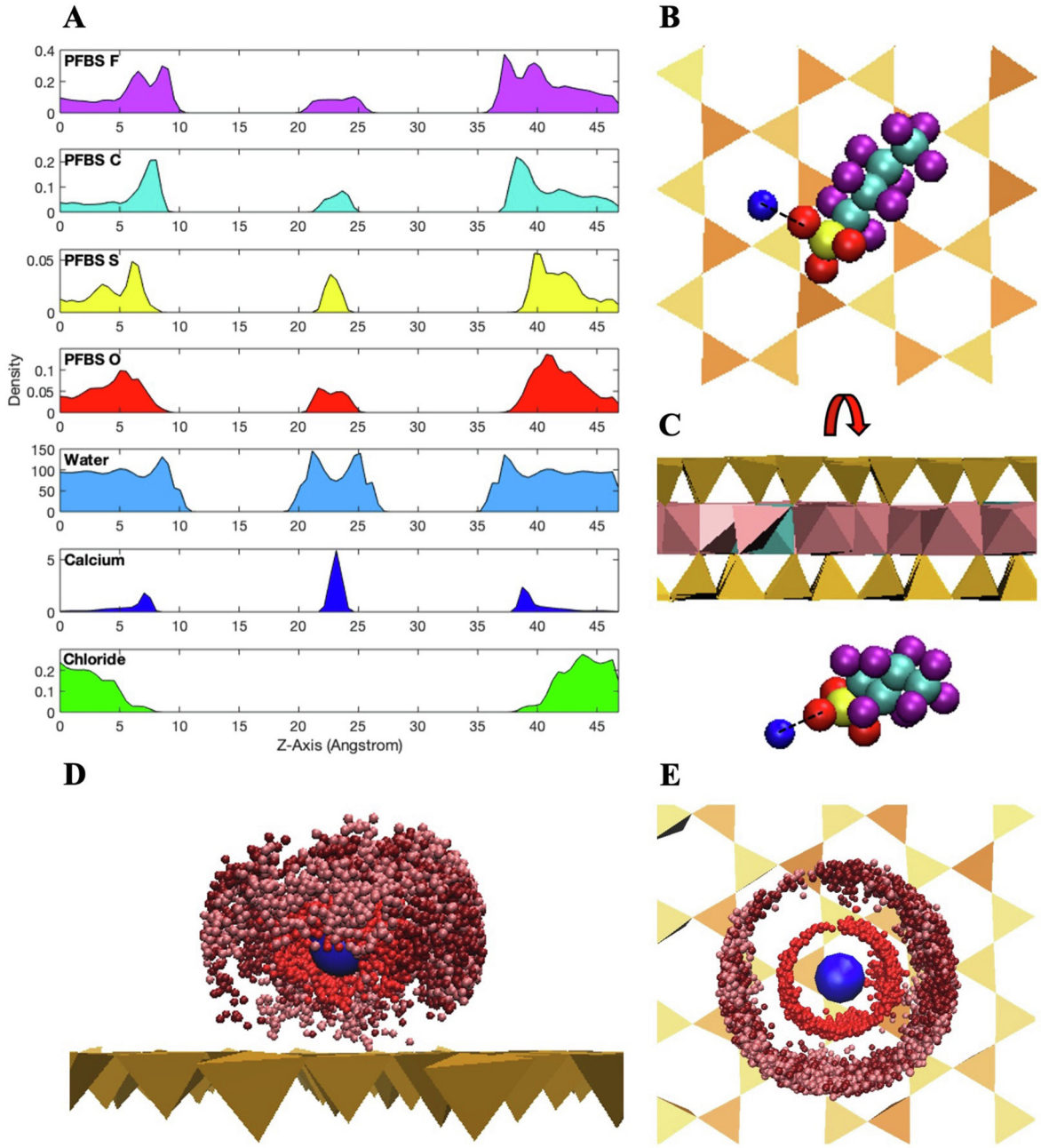

Fig. 4. (A) Atomic density profiles of PFBS, water, calcium, and chloride in the clay region (defined in Fig. 2) as a function of *z* in the unbiased simulation at 0.1 M $CaCl_2$. (B–C) Two perspectives of a representative snapshot of an adsorbed PFBS molecule in the same system lying parallel to the lower basal surface. The CF chain (light blue and purple spheres) lies flat on the surface while the SO_3^- group (yellow and red spheres) orients towards a calcium ion (dark blue sphere). Water molecules are not shown. (D–E) Two perspectives of the locations of PFBS oxygen atoms (light, medium, and dark red spheres) relative to the location of a Ca^{2+} ion (blue sphere) on the exterior smectite basal surface. Different shades of red represent the location of sulfonate O atoms sampled at 1 ps intervals during 2 ns of the unbiased simulation. One of the sulfonate O atoms (medium red spheres) was consistently located ~2.3 Å from the Ca^{2+} ion during the sampled trajectory, while the other two sulfonate O atoms (dark and light red spheres) were located ~4.5 Å from Ca^{2+}. (For interpretation of the references to colour in this figure legend, the reader is referred to the web version of this article.)

examination of MD simulation snapshots reveals that the SO_3^- group tends to coordinate with Ca^{2+} (Fig. 4B–E). This observed 'lateral cation bridging' is predominantly mono-dentate (Fig. 4D–E) with the oxygen atoms occupying the same plane as the calcium ions (relative to the clay basal surface), while the hydrophobic CF chain remains on the mineral surface. Chloride ions are strongly excluded from the vicinity of the clay surface, in agreement with previous studies [89,90], indicating that the presence of the sulfonate group near the clay surface is generally unfavorable (from a mean field electrostatic perspective) despite its association with adsorbed Ca^{2+}. Similar density profiles were observed at other aqueous chemistry conditions as shown in Fig. S1. Overall, our results support the hypothesis that Ca^{2+} significantly enhances the affinity of smectite for anionic organic compounds—which is thought to play an important role, for example, in the dynamics of soil organic matter [79–82] but the details of the interaction observed here differ from the canonical view: first, the Ca^{2+} ions in our study do not physically 'bridge' the mineral surface and the organic compounds and, second, favorable Ca-organic Coulomb interactions do not drive the adsorption phenomenon; instead, they minimize the overall Coulomb repulsion and, therefore, facilitate the expression of the entropy-driven hydrophobic adsorption.

3.4. Energetics of PFBS adsorption

The average potential energies of adsorbed and non-adsorbed PFBS molecules in the unbiased simulations were calculated from the pairwise interaction energies of PFBS molecules with all other species in the simulation cell. Results are presented in Fig. 5 as the VdW and Coulomb contributions to the potential energy of PFBS in the bulk-liquid-like water region and on the lower basal surface. In all cases, VdW interactions are small and almost identical in the bulk liquid and surface regions. Based on the difference between these interactions in the bulk liquid and surface regions, their contribution to the overall enthalpy of adsorption is <0.02 eV. Coulomb interactions constitute the majority of the total pairwise interactions, as expected given the charged nature of PFBS. The difference between the Coulomb interactions in bulk water and on the lower basal surface is consistently unfavorable to adsorption, as expected due to the anionic nature of PFBS. The magnitude of this unfavorable contribution was greater (by ~0.1 eV) in the systems containing monovalent cations (0.18 ± 0.02 eV) than in the system containing calcium (0.07 ± 0.03 eV). A decomposition of the combined VdW and Coulomb pairwise interactions near the lower clay surface indicates that the vast majority of the contribution comes from favorable PFBS-water (58.3–83.5%) and PFBS-cation (13.0–37.2%) interactions with small unfavorable contributions from PFBS-clay (3.4–3.9%), PFBS-chloride (<0.1–2.8%), and PFBS-PFBS interactions (<0.1–0.2%). In short, the potential energy of adsorbed PFBS is dominated by interactions with surface water and cations, rather than with the clay structure. The very small PFBS-PFBS interaction term along with a visual inspection of simulation trajectories indicates that at the simulated concentration (1.66 mM), aggregation is not an important adsorption mechanism. At significantly higher concentrations, aggregation may become important as accessible adsorption domains become occupied.

The enthalpy of adsorption, ΔH_{ads}, can be closely approximated as the difference between the potential energies of interaction of the solute with its surroundings in the clay region vs. the bulk liquid water if the small difference in intramolecular interactions in these two regions are neglected. Enthalpies of adsorption estimated in this manner are shown in Fig. 5 for PFBS on the lower clay basal surface at all five aqueous chemistry conditions examined in this study. The results indicate that the enthalpic contribution to adsorption is unfavorable in all cases. The enthalpy of adsorption is less unfavorable in the case of $CaCl_2$ (0.09 ± 0.04 eV) relative to the other conditions (0.16 ± 0.02 eV on average) due to enhanced favorability of interactions with calcium ions near the clay surface. The identical enthalpies of adsorption in 0.1 M KCl vs. NaCl solutions confirm that the enhanced adsorption in the presence of K^+ is an entropic effect, as hypothesized in previous studies [48,83,84] and in agreement with measurements showing similar adsorption of DNA on the basal surface of K- vs. Na-exchanged mica (a surface isostructural to that of smectite but with much smaller uncharged surface patches) [91]. In all cases, the unfavorable enthalpy of adsorption derives predominately from differences in electrostatic interactions between PFBS and water molecules in the two regions. Specifically, PFBS-water Coulomb interactions are less favorable in the vicinity of the clay surface than in bulk liquid water (Fig. 6), in agreement with previous research on anion exclusion [92]. This is particularly evident within the interlayer region as unfavorable interactions with water, and to a lesser extent the clay surfaces, relative to the bulk region result in the unfavorable enthalpy of adsorption that makes intercalation only slightly favorable (in the case of $CaCl_2$) or unfavorable (in the case of NaCl or KCl) (Fig. S2).

The entropic contribution to adsorption, $-T\Delta S_{ads}$, can be estimated from ΔH_{ads} and the free energy of partitioning to the water within the defined adsorption region, $\Delta F_{ads} = -RT\ln(K_d \times M_{clay}/V_{water\_in\_clay} + 1)$, where the K_d values are those reported in Table 1 and M_{clay} and $V_{water\_in\_clay}$ represent the mass of clay and volume of water in the region defined as the adsorption domain [39]. This calculation assumes that the small term relating the Helmholtz and Gibbs free energies is negligible due to the inclusion of an NPT equilibration step at P = 1 bar. The results, shown in Fig. 5, indicate that PFBS adsorption is driven by favorable entropic contributions to the free energy of adsorption in all aqueous chemistry conditions tested. This corroborates our observation that PFBS adsorption occurs predominantly on uncharged hydrophobic patches of the smectite surface (Fig. 3).

3.5. Effects of PFAS chain length

A similar analysis was performed to compare PFBS, PFHxS, and PFOS adsorption in $CaCl_2$. Metadynamics results, shown in Fig. S3, once again show significant adsorption on the lower basal surface with calculated log K_d values of 3.5 ± 0.4, 3.4 ± 0.8, and 5.8 ± 1.1 for PFBS, PFHxS and PFOS respectively. PFHxS adsorption predominately occurred on the largest uncharged patch and PFOS adsorption was exclusively on this domain (Fig. S4). As expected, the component of PFAS potential energy associated with VdW interactions increases slightly with increasing molecular size, while the difference between VdW interactions in bulk water and on the clay

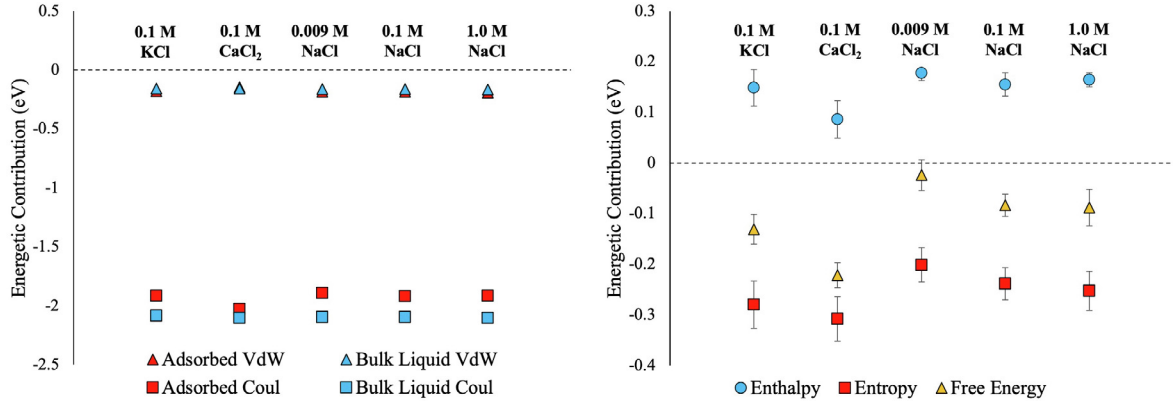

Fig. 5. Left: Average VdW (triangles) and Coulomb (squares) interactions between PFBS and all other species in the simulated system for organic molecules located on the lower basal surface (red) or in the bulk-liquid-like region (blue). The 95% confidence intervals range from <0.01 to 0.04 eV. Right: Enthalpic (blue circles) and entropic (red squares) contributions to the free energy of adsorption (yellow triangles) on the lower basal surface. Error bars represent 95% confidence intervals. The reported entropy refers to the $-T\Delta S$ contribution to the free energy of adsorption. (For interpretation of the references to colour in this figure legend, the reader is referred to the web version of this article.)

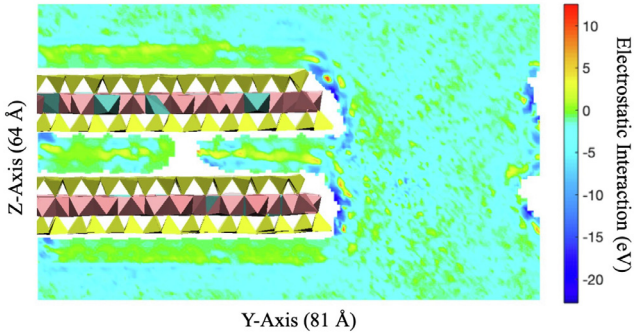

Fig. 6. Map of the average PFBS-water Coulomb interaction energy averaged over 85 ns of an unbiased simulation in the system with 0.1 M $CaCl_2$. Results are averaged over all PFBS atoms, then multiplied by 17 so that their scale is comparable to that of the per-molecule energies shown in previous figures. The white region in the interlayer was not explored by PFBS molecules during the unbiased simulation.

surface (i.e., the contribution of VdW interactions to adsorption) remains small (Fig. 7). Interestingly, the contribution of Coulomb interactions to adsorption was significantly less unfavorable (by ~0.1 eV) for PFBS than for PFHxS or PFOS, contrary to the expectation that Coulomb interactions would be unchanged with the addition of CF_2 groups. We hypothesize that this difference manifests from the ability of the PFBS molecule to occupy the smaller uncharged patches on the clay surface (as shown in Fig. 3). In other words, the smaller size of PFBS may allow it to access additional hydrophobic sites, including sites where it interacts more favorably with adsorbed Ca^{2+} ions.

The energetic breakdown into enthalpic and entropic components is shown in Fig. 7. The enthalpic contribution to adsorption is unfavorable in all cases, but significantly less so in the case of PFBS due to the aforementioned enhanced interactions with Ca^{2+} in the clay region in comparison to PFHxS and PFOS. The entropic contribution increases linearly (R^2 = 0.82) with increasing chain length, with a favorable entropic change of −0.06 ± 0.02 eV for each additional CF_2 group. Previous estimates of the entropy of solvation associated with the addition of a CH_2 group to an organic compound (~0.04 eV) and the entropy associated with the transformation of a CH_2 group to CF_2 (~0.04 eV) can be combined to approximate the entropy of solvation associated with the addition of a CF_2 group to an organic compound in bulk liquid water [93,94]. This estimate (~0.08 eV) is consistent with our results and suggests that the increased adsorption of longer chained PFAS molecules stems from their decreased solubility in bulk liquid water. Additionally, our reported trend is of similar magnitude to experimental observations that the free energy of adsorption of PFASs on sediments and kaolinite varies by ~−0.03 eV per CF_2 group for compounds with 6 to 10 perfluorinated carbon atoms [21,30]. Combined, these results indicate that the adsorption of long-chain PFASs is driven by favorable entropic contributions to the adsorption free energy that increase linearly with compound size. However, our results also suggest a qualitative change in behavior in the case of short-chain PFASs (such as PFBS) whereby the enthalpic contribution to adsorption becomes less unfavorable, with the result that the short-chain compounds adsorb more strongly than expected.

4. Conclusions

MD simulations were used to elucidate the fundamental mechanisms and thermodynamics of PFBS, PFHxS, and PFOS adsorption by smectite clay minerals. Adsorption was observed in all simulated systems and was most favorable in the presence of Ca^{2+}. Clay surface charge density was a major factor governing the extent of adsorption as PFAS density was concentrated on the less charged smectite lamella. Hydrophobic patches spatially distant from the smectite isomorphic substitutions were identified as the primary adsorption domains, confirming a hypothesis formulated from previous experimental results [38,87]. On these patches, the hydrophobic CF tail was able to displace the first layer of water molecules forming an inner-sphere complex with the surface. The longer PFHxS and PFOS molecules were sterically limited to the larger adsorption domains.

Metadynamics simulations were used to calculate the free energy of adsorption and complementary unbiased simulations were used to determine the enthalpy of adsorption. The enthalpy of adsorption was unfavorable in all systems due primarily to less favorable PFAS-water interactions in the adsorbed region relative to the bulk aqueous region. For PFBS, the enthalpy of adsorption was less unfavorable in the presence of Ca^{2+} due to stabilizing lateral cation bridging interactions between the negatively charged sulfonate head group and divalent cations. The entropy of adsorption was estimated as the difference of the enthalpy and free energy of adsorption. The entropic contribution to adsorption increased linearly with increasing CF chain length and was found to be the driving force for PFAS adsorption, in agreement with the observation that adsorption occurs on the hydrophobic patches of the smectite surface.

The results presented in this paper highlight several exciting paths for future study. In particular, the discovery of the importance of hydrophobic partitioning for PFAS adsorption on clay minerals points to kaolinite, low-charge smectite, and organoclays as

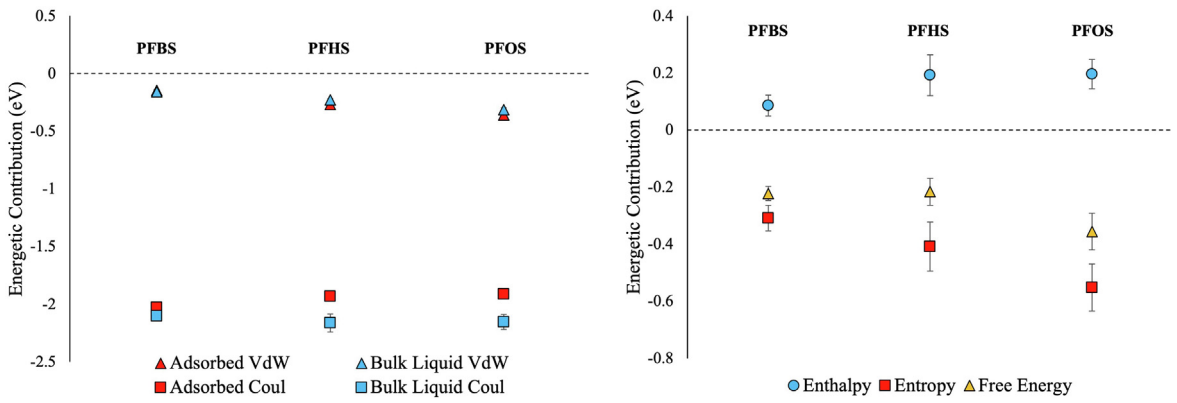

Fig. 7. Same as Fig. 5 in the case of the adsorption of PFBS, PFHxS, and PFOS on the lower basal surface in 0.1 M $CaCl_2$. The 95% confidence intervals range from <0.01 to 0.09 eV.

promising candidates for adsorbent studies. In addition, the demonstration that surface charge density strongly influences adsorption suggests a need for systematic study of adsorption on smectite and other minerals with differing layer charges and isomorphic substitution patterns. Furthermore, the demonstration of different PFAS affinities for internal vs. external basal surfaces suggests that the impact of clay aggregation on adsorption represents an opportunity for future research.

CRediT authorship contribution statement

Jennifer A.R. Willemsen: Conceptualization, Methodology, Investigation, Visualization, Writing - original draft. **Ian C. Bourg:** Supervision, Funding acquisition, Writing - review & editing.

Declaration of Competing Interest

The authors declare that they have no known competing financial interests or personal relationships that could have appeared to influence the work reported in this paper.

Acknowledgements

This material is based upon work supported by the U.S. National Science Foundation under Grant No. CBET 1931611. Additional support was provided by the U.S. Department of Energy, Office of Basic Energy Sciences, Geosciences Program under Award DE-SC0018419 and by the High Meadows Environmental Institute through the Carbon Mitigation Initiative and the Mary and Randall Hack '69 Graduate Award for Water and the Environment. Molecular dynamics simulations were performed using resources of the National Energy Research Scientific Computing Center (NERSC), which is supported by the U.S. Department of Energy, Office of Sciences, under Award DE-AC02-05CH11231.

Appendix A. Supplementary material

Supplementary data to this article can be found online at https://doi.org/10.1016/j.jcis.2020.11.071.

References

[1] S. Kar, M.S. Sepúlveda, K. Roy, J. Leszczynski, Endocrine-Disrupting Activity of Per- and Polyfluoroalkyl Substances: Exploring Combined Approaches of Ligand and Structure Based Modeling, Chemosphere 184 (2017) 514–523.
[2] K. Steenland, S. Woskie, Cohort Mortality Study of Workers Exposed to Perfluorooctanoic Acid, Am. J. Epidemiol. 176 (2012) 909–917.
[3] V.M. Vieira, K. Hoffman, H.-M. Shin, J.M. Weinberg, T.F. Webster, T. Fletcher, Perfluorooctanoic Acid Exposure and Cancer Outcomes in a Contaminated Community: A Geographic Analysis, Environ. Health Perspect. 121 (2013) 318–323.
[4] J.C. DeWitt, M.M. Peden-Adams, J.M. Keller, D.R. Germolec, Immunotoxicity of Perfluorinated Compounds: Recent Developments, Toxicol. Pathol. 40 (2012) 300–311.
[5] Z. Liew, H. Goudarzi, Y. Oulhote, Developmental Exposures to Perfluoroalkyl Substances (PFASs): An Update of Associated Health Outcomes, Curr. Environ. Health Rpt. 5 (2018) 1–19.
[6] C. Fei, J.K. McLaughlin, R.E. Tarone, J. Olsen, Perfluorinated Chemicals and Fetal Growth: A Study Within the Danish National Birth Cohort, Environ. Health Perspect. 115 (2007) 1677–1682.
[7] C. Fei, J.K. McLaughlin, L. Lipworth, J. Olsen, Prenatal Exposure to Perfluorooctanoate (PFOA) and Perfluorooctanesulfonate (PFOS) and Maternally Reported Developmental Milestones in Infancy, Environ. Health Perspect. 116 (2008) 1391–1395.
[8] A.B. Lindstrom, M.J. Strynar, E.L. Libelo, Polyfluorinated Compounds: Past, Present, and Future, Environ. Sci. Technol. 45 (2011) 7954–7961.
[9] A.M. Calafat, L.-Y. Wong, Z. Kuklenyik, J.A. Reidy, L.L. Needham, Polyfluoroalkyl Chemicals in the U.S. Population: Data from the National Health and Nutrition Examination Survey (NHANES) 2003–2004 and Comparisons with NHANES 1999–2000, Environ. Health Perspect. 115 (2007) 1596–1602.
[10] A. Cordner, V.Y. De La Rosa, L.A. Schaider, R.A. Rudel, L. Richter, P. Brown, Guideline Levels for PFOA and PFOS in Drinking Water: The Role of Scientific Uncertainty, Risk Assessment Decisions, and Social Factors, J. Exposure Sci. Environ. Epidemiol. 29 (2019) 157–171.
[11] S. Liu, R. Yang, N. Yin, F. Faiola, The Short-Chain Perfluorinated Compounds PFBS, PFHxS, PFBA and PFHxA, Disrupt Human Mesenchymal Stem Cell Self-Renewal and Adipogenic Differentiation, J. Environ. Sci. 88 (2020) 187–199.
[12] M. Nian, K. Luo, F. Luo, R. Aimuzi, X. Huo, Q. Chen, Y. Tian, J. Zhang, Association Between Prenatal Exposure to PFAS and Fetal Sex Hormones: Are the Short-Chain PFAS Safer?, Environ. Sci. Technol. 54 (2020) 8291–8299.
[13] R. Vestergren, I.T. Cousins, Tracking the Pathways of Human Exposure to Perfluorocarboxylates, Environ. Sci. Technol. 43 (2009) 5565–5575.
[14] H. Fromme, S.A. Tittlemier, W. Völkel, M. Wilhelm, D. Twardella, Perfluorinated Compounds – Exposure Assessment for the General Population in Western Countries, Int. J. Hyg. Environ. Health 212 (2009) 239–270.
[15] C. Eschauzier, E. Beerendonk, P. Scholte-Veenendaal, P. De Voogt, Impact of Treatment Processes on the Removal of Perfluoroalkyl Acids from the Drinking Water Production Chain, Environ. Sci. Technol. 46 (2012) 1708–1715.
[16] X.C. Hu, D.Q. Andrews, A.B. Lindstrom, T.A. Bruton, L.A. Schaider, P. Grandjean, R. Lohmann, C.C. Carignan, A. Blum, S.A. Balan, C.P. Higgins, E.M. Sunderland, Detection of Poly- and Perfluoroalkyl Substances (PFASs) in U.S. Drinking Water Linked to Industrial Sites, Military Fire Training Areas, and Wastewater Treatment Plants, Environ. Sci. Technol. Lett. 3 (2016) 344–350.
[17] S.W. Karickhoff, Organic Pollutant Sorption in Aquatic Systems, J. Hydraul. Eng. 110 (1984) 707–735.
[18] W.J. Weber Jr., P.M. McGinley, L.E. Katz, Sorption Phenomena in Subsurface Systems: Concepts, Models, and Effects on Contaminant Fate and Transport, Water Res. 25 (1991) 499–528.
[19] S.A. Boyd, G. Sheng, B.J. Teppen, C.T. Johnston, Mechanisms for the Adsorption of Substituted Nitrobenzenes by Smectite Clays, Environ. Sci. Technol. 35 (2001) 4227–4234.
[20] M.L. Ferrey, J.T. Wilson, C. Adair, C. Su, D.D. Fine, X. Liu, J.W. Washington, Behavior and Fate of PFOA and PFOS in Sandy Aquifer Sediment, Ground Water Monit. Rem. 32 (2012) 63–71.
[21] C.P. Higgins, R.G. Luthy, Sorption of Perfluorinated Surfactants on Sediments, Environ. Sci. Technol. 40 (2006) 7251–7256.
[22] R.L. Johnson, A.J. Anschutz, J.M. Smolen, M.F. Simcik, R.L. Penn, The Adsorption of Perfluorooctane Sulfonate onto Sand, Clay, and Iron Oxide Surfaces, J. Chem. Eng. Data 52 (2007) 1165–1170.
[23] J. Lehmann, M. Kleber, The Contentious Nature of Soil Organic Matter, Nature 528 (2015) 60–69.
[24] D. Petrov, D. Tunega, M.H. Gerzabek, C. Oostenbrink, Molecular Dynamics Simulations of the Standard Leonardite Humic Acid: Microscopic Analysis of the Structure and Dynamics, Environ. Sci. Technol. 51 (2017) 5414–5424.
[25] J. Jeon, K. Kannan, B.J. Lim, K.G. An, S.D. Kim, Effects of Salinity and Organic Matter on the Partitioning of Perfluoroalkyl Acid (PFAs) to Clay Particles, J. Environ. Monit. 13 (2011) 1803–1810.
[26] H. Tian, J. Gao, H. Li, S.A. Boyd, C. Gu, Complete Defluorination of Perfluorinated Compounds by Hydrated Electrons Generated from 3-Indole-Acetic-Acid in Organomodified Montmorillonite, Sci. Rep. 6 (2016) 32949.
[27] R. Zhang, W. Yan, C. Jing, Mechanistic Study of PFOS Adsorption on Kaolinite and Montmorillonite, Colloids Surf. A: Physicochem. Eng. Aspects 462 (2014) 252–258.
[28] L. Zhao, J. Bian, Y. Zhang, L. Zhu, Z. Liu, Comparison of the Sorption Behaviors and Mechanisms of Perfluorosulfonates and Perfluorocarboxylic Acids on Three Kinds of Clay Minerals, Chemosphere 114 (2014) 51–58.
[29] Q. Zhou, S. Deng, Q. Yu, Q. Zhang, G. Yu, J. Huang, H. He, Sorption of Perfluorooctane Sulfonate on Organo-Montmorillonites, Chemosphere 78 (2010) 688–694.
[30] F. Xiao, X. Zhang, L. Penn, J.S. Gulliver, M.F. Simcik, Effects of Monovalent Cations on the Competitive Adsorption of Perfluoroalkyl Acids by Kaolinite: Experimental Studies and Modeling, Environ. Sci. Technol. 45 (2011) 10028–10035.
[31] C.Y. Tang, Q.S. Fu, D. Gao, C.S. Criddle, J.O. Leckie, Effect of Solution Chemistry on the Adsorption of Perfluorooctane Sulfonate onto Mineral Surfaces, Water Res. 2010 (44) (2010) 2654–2662.
[32] F. Wang, K. Shih, Adsorption of Perfluorooctanesulfonate (PFOS) and Perfluorooctanoate (PFOA) on Alumina: Influence of Solution pH and Cations, Water Res. 45 (2011) 2925–2930.
[33] L. Ahrens, L.W.Y. Yeung, S. Taniyasu, P.K.S. Lam, N. Yamashita, Partitioning of Perfluorooctanoate (PFOA), Perfluorooctane Sulfonate (PFOS) and Perfluorooctane Sulfonamide (PFOSA) Between Water and Sediment, Chemosphere 85 (2011) 731–737.
[34] J.L. Guelfo, C.P. Higgins, Subsurface Transport Potential of Perfluoroalkyl Acids at Aqueous Film-Forming Foam (AFFF)-Impacted Sites, Environ. Sci. Technol. 47 (2013) 4164–4171.
[35] R. Zhang, W. Yan, C. Jing, Experimental and Molecular Dynamic Simulation Study of Perfluorooctane Sulfonate Adsoption on Soil and Sediment Components, J. Environ. Sci. 29 (2015) 131–138.
[36] N. Merino, Y. Qu, R.A. Deeb, E.L. Hawley, M.R. Hoffmann, S. Mahendra, Degradation and Removal Methods for Perfluoroalkyl and Polyfluoroalkyl Substances in Water, Environ. Eng. Sci. 33 (2016) 615–649.
[37] Z. Du, S. Deng, Y. Bei, Q. Huang, B. Wang, J. Huang, G. Yu, Adorption Behavior and Mechanism of Perfluorinated Compounds on Various Adsorbents - A Review, J. Hazard. Mater. 274 (2014) 443–454.
[38] K.W. Weissmahr, S.B. Haderlein, R.P. Schwarzenbach, Complex Formation of Soil Minerals with Nitroaromatic Explosives and Other π-Acceptors, Soil Sci. Soc. Am. J. 62 (1998) 369–378.

[39] J.A.R. Willemsen, S.C.B. Myneni, I.C. Bourg, Molecular Dynamics Simulations of the Adsorption of Phthalate Esters on Smectite Clay Surfaces, J. Phys. Chem. C 123 (2019) 13624–13636.
[40] J.R. Ray, I.A. Shabtai, M. Teixidó, Y.G. Mishael, D.L. Sedlak, Polymer-Clay Composite Geomedia for Sorptive Removal of Trace Organic Compounds and Metals in Urban Stormwater, Water Res. 157 (2019) 454–462.
[41] B. Yan, G. Munoz, S. Sauvé, J. Liu, Molecular Mechanisms of Per- and Polyfluoroalkyl Substances on a Modified Clay: A Combined Experimental and Molecular Simulation Study, Water Res. 184 (2020) 116166.
[42] V. Aggarwal, Y.-Y. Chien, B.J. Teppen, Molecular Simulations to Estimate Thermodynamics for Adsorption of Polar Organic Solutes to Montmorillonite, Eur. J. Soil Sci. 58 (2007) 945–957.
[43] L. Aristilde, C. Marichal, J. Miéhé-Brendlé, B. Lanson, L. Charlet, Interactions of Oxytetracycline with a Smectite Clay: A Spectroscopic Study with Molecular Simulations, Environ. Sci. Technol. 44 (2010) 7839–7845.
[44] L. Aristilde, B. Lanson, J. Miéhé-Brendlé, C. Marichal, L. Charlet, Enhanced Interlayer Trapping of a Tetracycline Antibiotic Within Montmorillonite Layers in the Presence of Ca and Mg, J. Colloid Interface Sci. 464 (2016) 153–159.
[45] M.A. Chappell, D.A. Laird, M.L. Thompson, H. Li, B.J. Teppen, V. Aggarwal, C.T. Johnston, S.A. Boyd, Influence of Smectite Hydration and Swelling on Atrazine Sorption Behavior, Environ. Sci. Technol. 39 (2005) 3150–3156.
[46] F.E.K. Okaikue-Woodi, S.E. Kelch, M.P. Schmidt, C.E. Martinez, R.E. Youngman, L. Aristilde, Structures and Mechanisms in Clay Nanopore Trapping of Structurally-Different Fluoroquinolone Antimicrobials, J. Colloid Interface Sci. 513 (2018) 367–378.
[47] M. Samaraweera, W. Jolin, D. Vasudevan, A.A. Mackay, J.A. Gascón, Atomistic Prediction of Sorption Free Energies of Cationic Aromatic Amines on Montmorillonite: A Linear Interaction Energy Method, Environ. Sci. Technol. Lett. 1 (2014) 284–289.
[48] G. Sheng, C.T. Johnston, B.J. Teppen, S.A. Boyd, Adsorption of Dinitrophenol Herbicides from Water by Montmorillonites, Clays Clay Miner. 50 (2002) 25–34.
[49] Q. Zhou, R. Zhu, S.C. Parker, J. Zhu, H. He, M. Molinari, Modelling the Effects of Surfactant Loading Level on the Sorption of Organic Contaminants on Organoclays, RSC Adv. 5 (2015) 47022–47030.
[50] C. Liu, C. Gu, K. Yu, H. Li, B.J. Teppen, C.T. Johnston, S.A. Boyd, D. Zhou, Integrating Structural and Thermodynamic Mechanisms for Sorption of PCBs by Montmorillonite, Environ. Sci. Technol. 49 (2015) 2796–2805.
[51] T.V. Shapley, M. Molinari, R. Zhu, S.C. Parker, Atomistic Modeling of the Sorption Free Energy of Dioxins at Clay– Water Interfaces, J. Phys. Chem. C 117 (2013) 24975–24984.
[52] D. Tunega, M.H. Gerzabek, G. Haberhauer, H. Lischka, R. Solc, A.J.A. Aquino, Adsorption Process of Polar and Nonpolar Compounds in a Nanopore Model of Humic Substances, Eur. J. Soil Sci. (2019) 1–11.
[53] B. Ensing, A. Laio, M. Parrinello, M.L. Klein, A Recipe for the Computation of the Free Energy Barrier and the Lowest Free Energy Path of Concerted Reactions, J. Phys. Chem. B 109 (2005) 6676–6687.
[54] B. Ensing, M. De Vivo, Z. Liu, P. Moore, M.L. Klein, Metadynamics as a Tool for Exploring Free Energy Landscapes of Chemical Reactions, Acc. Chem. Res. 39 (2006) 73–81.
[55] A. Laio, F.L. Gervasio, Metadynamics: A Method to Simulate Rare Events and Reconstruct the Free Energy in Biophysics, Chemistry and Material Science, Rep. Prog. Phys. 71 (2008) 126601.
[56] A. Laio, M. Parrinello, Escaping Free-Energy Minima, Proc. Natl. Acad. Sci. 99 (2002) 12562–12566.
[57] I.C. Bourg, S.S. Lee, P. Fenter, C. Tournassat, Stern Layer Structure and Energetics at Mica–Water Interfaces, J. Phys. Chem. C 121 (2017) 9402–9412.
[58] I.C. Bourg, G. Sposito, Connecting the Molecular Scale to the Continuum Scale for Diffusion Processes in Smectite-Rich Porous Media, Environ. Sci. Technol. 44 (2010) 2085–2091.
[59] R.T. Cygan, S. Guggenheim, A.F. Koster Van Groos, Molecular Models for the Intercalation of Methane Hydrate Complexes in Montmorillonite Clay, J. Phys. Chem. B 108 (2004) 15141–15149.
[60] M. Holmboe, I.C. Bourg, Molecular Dynamics Simulations of Water and Sodium Diffusion in Smectite Interlayer Nanopores as a Function of Pore Size and Temperature, J. Phys. Chem. C 118 (2014) 1001–1013.
[61] G. Hura, D. Russo, R.M. Glaeser, T. Head-Gordon, M. Krack, M. Parrinello, Water Structure as a Function of Temperature from X-ray Scattering Experiments and *Ab Initio* Molecular Dynamics, Phys. Chem. Chem. Phys. 5 (2003) 1981–1991.
[62] G. Sposito, N.T. Skipper, R. Sutton, S.-H. Park, A.K. Soper, J.A. Greathouse, Surface Geochemistry of the Clay Minerals, Proc. Natl. Acad. Sci. 96 (1999) 3358–3364.
[63] S. Plimpton, Fast Parallel Algorithms for Short-Range Molecular Dynamics, J. Comput. Phys. 117 (1995) 1–19.
[64] G. Fiorin, M.L. Klein, J. Hénin, Using Collective Variables to Drive Molecular Dynamics Simulations, Mol. Phys. 111 (2013) 3345–3362.
[65] R.T. Cygan, J.-J. Liang, A.G. Kalinichev, Molecular Models of Hydroxide, Oxyhydroxide, and Clay Phases and the Development of a General Force Field, J. Phys. Chem. B 108 (2004) 1255–1266.
[66] L.N. Lammers, I.C. Bourg, M. Okumura, K. Kolluri, G. Sposito, M. Machida, Molecular Dynamics Simulations of Cesium Adsorption on Illite Nanoparticles, J. Colloid Interface Sci. 490 (2017) 608–620.
[67] W.L. Jorgensen, D.S. Maxwell, J. Tirado-Rives, Development and Testing of the OPLS All-Atom Force Field on Conformational Energetics and Properties of Organic Liquids, J. Am. Chem. Soc. 118 (1996) 11225–11236.
[68] J.N.C. Lopes, A.A.H. Pádua, Molecular Force Field for Ionic Liquids Composed of Triflate or Bistriflylimide Anions, J. Phys. Chem. B 108 (2004) 16893–16898.
[69] H.J.C. Berendsen, J.R. Grigera, T.P. Straatsma, The Missing Term in Effective Pair Potentials, J. Phys. Chem. 91 (1987) 6269–6271.
[70] J. Åqvist, Ion-Water Interaction Potentials Derived from Free Energy Perturbation Simulations, J. Phys. Chem. 94 (1990) 8021–8024.
[71] D.E. Smith, L.X. Dang, Computer Simulations of NaCl Association in Polarizable Water, J. Chem. Phys. 100 (1994) 3757–3766.
[72] L.X. Dang, Mechanism and Thermodynamics of Ion Selectivity in Aqueous Solutions of 18-Crown-6 Ether: A Molecular Dynamics Study, J. Am. Chem. Soc. 117 (1995) 6954–6960.
[73] J.W. Eastwood, R.W. Hockney, D.N. Lawrence, P3M3DP – The Three-Dimensional Periodic Particle-Particle/Particle-Mesh Program, Comput. Phys. Commun. 19 (1980) 215–261.
[74] J.-P. Ryckaert, G. Ciccotti, H.J.C. Berendsen, Numerical Integration of the Cartesian Equations of Motion of a System with Constraints: Molecular Dynamics of *n*-Alkanes, J. Comput. Phys. 23 (1977) 327–341.
[75] W. Humphrey, A. Dalke, K. Schulten, VMD: Visual Molecular Dynamics, J. Mol. Graphics 14 (1996) 33–38.
[76] T.S. Arnarson, R.G. Keil, Mechanisms of Pore Water Organic Matter Adsorption to Montmorillonite, Mar. Chem. 71 (2000) 309–320.
[77] K.M. Dontsova, J.M. Bigham, Anionic Polysaccharide Sorption by Clay Minerals, Soil Sci. Soc. Am. J. 69 (2005) 1026–1035.
[78] R.A. Figueroa, A. Leonard, A.A. Mackay, Modeling Tetracycline Antibiotic Sorption to Clays, Environ. Sci. Technol. 38 (2004) 476–483.
[79] C. Chen, J.J. Dynes, J. Wang, C. Karunakaran, D.L. Sparks, Soft X-Ray Spectromicroscopy Study of Mineral-Organic Matter Associations in Pasture Soil Clay Fractions, Environ. Sci. Technol. 48 (2014) 6678–6686.
[80] R. Mikutta, C. Mikutta, K. Kalbitz, T. Scheel, K. Kaiser, R. Jahn, Biodegradation of Forest Floor Organic Matter Bound to Minerals via Different Binding Mechanisms, Geochim. Cosmochim. Acta 71 (2007) 2569–2590.
[81] J.M. Oades, The Retention of Organic Matter in Soils, Biogeochemistry 5 (1988) 35–70.
[82] R. Sutton, G. Sposito, Molecular Simulation of Humic Substance-Ca-Montmorillonite Complexes, Geochim. Cosmochim. Acta 70 (2006) 3566–3581.
[83] S.B. Haderlein, K.W. Weissmahr, R.P. Schwarzenbach, Specific Adsorption of Nitroaromatic Explosives and Pesticides to Clay Minerals, Environ. Sci. Technol. 30 (1996) 612–622.
[84] E. Hu, X. Zhao, S. Pan, Z. Ye, F. He, Sorption of Non-ionic Aromatic Organics to Mineral Micropores: Interactive Effect of Cation Hydration and Mineral Charge Density, Environ. Sci. Technol. 53 (2019) 3067–3077.
[85] N. Bolan, B. Sarkar, Y. Yan, Q. Li, H. Wijesekara, K. Kannan, D.C.W. Tsang, M. Schauerte, J. Bosch, H. Noll, Y.S. Ok, K. Scheckel, J. Kumpiene, K. Gobindlal, M. Kah, J. Sperry, M.B. Kirkham, H. Wang, Y.F. Tsang, D. Hou, J. Rinklebe, Remediation of poly- and perfluoroalkyl substances (PFAS) contaminated soils – To mobilize or to immobilize or to degrade?, J. Hazard. Mater. 401 (2021) 123892.
[86] D.A. Laird, E. Barriuso, R.H. Dowdy, W.C. Koskinen, Adsorption of Atrazine on Smectites, Soil Sci. Soc. Am. J. 56 (1992) 62–67.
[87] W.F. Jaynes, S.A. Boyd, Hydrophobicity of Siloxane Surfaces in Smectites as Revealed by Aromatic Hydrocarbon Adsorption from Water, Clays Clay Miner. 39 (1991) 428–436.
[88] M. Szczerba, A.G. Kalinichev, M. Kowalik, Intrinsic Hydrophobicity of Smectite Basal Surfaces Quantitatively Probed by Molecular Dynamics Simulations, Appl. Clay Sci. 188 (2020) 105497.
[89] I.C. Bourg, G. Sposito, Molecular Dynamics Simulations of the Electrical Double Layer on Smectite Surfaces Contacting Concentrated Mixed Electrolyte (NaCl-$CaCl_2$) Solutions, J. Colloid Interface Sci. 360 (2011) 701–715.
[90] C. Tournassat, Y. Chapron, P. Leroy, M. Bizi, F. Boulahya, Comparison of Molecular Dynamics Simulations with Triple Layer and Modified Gouy-Chapman Models in a 0.1 M NaCl-Montmorillonite System, J. Colloid Interface Sci. 339 (2009) 533–541.
[91] H. Zhai, L. Wang, C.V. Putnis, Molecular-Scale Investigations Reveal Noncovalent Bonding Underlying the Adsorption of Environmental DNA on Mica, Environ. Sci. Technol. 53 (2019) 11251–11259.
[92] C. Tournassat, I.C. Bourg, M. Holmboe, G. Sposito, C.I. Steefel, Molecular Dynamics Simulations of Anion Exclusion in Clay Interlayer Nanopores, Clays Clay Miner. 64 (2016) 374–388.
[93] V.H. Dalvi, P.J. Rossky, Molecular Origins of Fluorocarbon Hydrophobicity, Proc. Natl. Acad. Sci. 107 (2010) 13603–13607.
[94] B.J. Teppen, V. Aggarwal, Thermodynamics of Organic Cation Exchange Selectivity in Smectites, Clays Clay Miner. 55 (2007) 119–130.